JACS
JOURNAL OF THE AMERICAN CHEMICAL SOCIETY
Article
Cite This: J. Am. Chem. Soc. 2017, 139, 17114-17119
pubs.acs.org/JACS

High Efficiency Near-Infrared and Semitransparent Non-Fullerene Acceptor Organic Photovoltaic Cells

Yongxi Li,[†] Jiu-Dong Lin,[‡] Xiaozhou Che,[†] Yue Qu,[†] Feng Liu,[§] Liang-Sheng Liao,*[,‡] and Stephen R. Forrest*[,†]

[†]Department of Electrical Engineering and Computer Science, University of Michigan, Ann Arbor, Michigan 48109, United States
[‡]Jiangsu Key Laboratory for Carbon-Based Functional Materials & Devices, Institute of Functional Nano & Soft Materials (FUNSOM), Soochow University, Suzhou, Jiangsu 215123, People's Republic of China
[§]Department of Physics and Astronomy, and Collaborative Innovation Center of IFSA (CICIFSA), Shanghai Jiaotong University, Shanghai 200240, People's Republic of China

Supporting Information

ABSTRACT: The absence of near-infrared (NIR) solar cells with high open circuit voltage (V_{oc}) and external quantum efficiency (*EQE*) has impeded progress toward achieving organic photovoltaic (OPV) power conversion efficiency *PCE* > 15%. Here we report a small energy gap (1.3 eV), chlorinated nonfullerene acceptor-based solar cell with *PCE* = 11.2 ± 0.4%, short circuit current of 22.5 ± 0.6 mA cm^{-2}, V_{oc} = 0.70 ± 0.01 V and fill factor of 0.71 ± 0.02, which is the highest performance reported to date for NIR single junction OPVs. Importantly, the *EQE* of this NIR solar cell reaches 75%, between 650 and 850 nm while leaving a transparency window between 400 and 600 nm. The semitransparent OPV using an ultrathin (10 nm) Ag cathode shows *PCE* = 7.1 ± 0.1%, with an average visible transmittance of 43 ± 2%, Commission d'Eclairage chromaticity coordinates of (0.29, 0.32) and a color rendering index of 91 for simulated AM1.5 illumination transmitted through the cell.

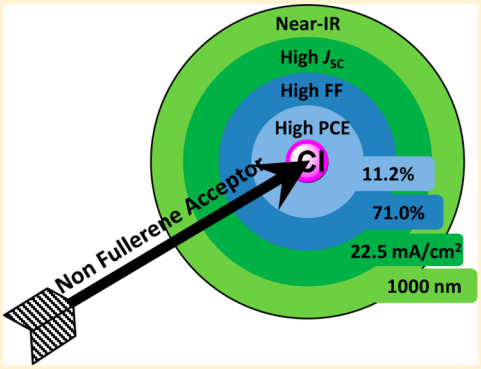

INTRODUCTION

Organic photovoltaics (OPVs) are an emerging technology with benefits such as potentially low cost materials and processes, flexibility, lightweight, semitransparency and compatibility with large-area manufacturing.[1] Over the past two decades, fullerene derivatives have been the dominant choice for electron acceptors,[2] leading to OPVs with power conversion efficiencies of *PCE* ~ 11%.[3] One challenge for the OPVs is the high energy loss in the conversion from the exciton to the intermediate charge transfer state that is the precursor to free charge generation.[4] By stacking both large and small energy-gap cells into a tandem OPV, the losses can be minimized.[5] By selectively absorbing visible and near-infrared (NIR) photons in separate elements in two-junction OPV cells with subcell energy gaps of 1.4 and 1.9 eV, it has been asserted that the cells can reach a *PCE* = 23%.[5c] However, the absence of small energy gap materials (<1.4 eV) with high open circuit voltage (V_{oc}) and external quantum efficiency (*EQE*) in the near-infrared (NIR)[6] has impeded progress toward achieving this goal. Considerable effort has therefore focused on developing small energy gap polymer and small molecule donors to overcome this deficiency.[7] Thus far, however, OPVs based on fullerene acceptors show only *PCE* < 10% with energy gap <1.4 eV.[6a] Particularly, most of these cells have *EQE* < 50%, which is insufficient to satisfy the requirements for a high efficiency tandem cell.

In addition to the pursuit of high device efficiency, OPVs have unique advantages, such as the application of semitransparent solar cells for use in building integrated photovoltaics (BIPV).[8] Considering the vast surface areas of windows and facades in modern urban environments, developing semitransparent solar cells (i.e., nearly transparent across the visible wavelengths from 400 to 650 nm) with both high efficiency and transmittance become increasingly important. For a solar cell to be highly transparent, visible light would have to be entirely transmitted. Selectively harvesting NIR radiation avoids competition between efficiency and transmittance. However, the lack of high performance NIR absorbers in conventional fullerene-based OPVs has prevented the attainment of efficient, yet highly transparent (in the visible) devices. To date, semitransparent OPVs based on fullerene acceptors show *PCE* ≤ 4% with average visible transmittance of 61%.[8a]

Rapid progress in developing small energy gap nonfullerene acceptors (NFAs) provides new opportunities to achieve both high efficiency and transparency.[9] However, most NFAs strongly absorb in the UV−vis range,[10] whereas NFAs with an absorption cutoff in the NIR region are rare.[11] Yao et al. reported acceptor-π-bridge-donor-π-bridge-acceptor (a-π-d-π-a) NFAs with absorption edges extending to ~1000 nm.[12] Due

Received: August 8, 2017
Published: November 16, 2017

DOI: 10.1021/jacs.7b11278
J. Am. Chem. Soc. 2017, 139, 17114−17119

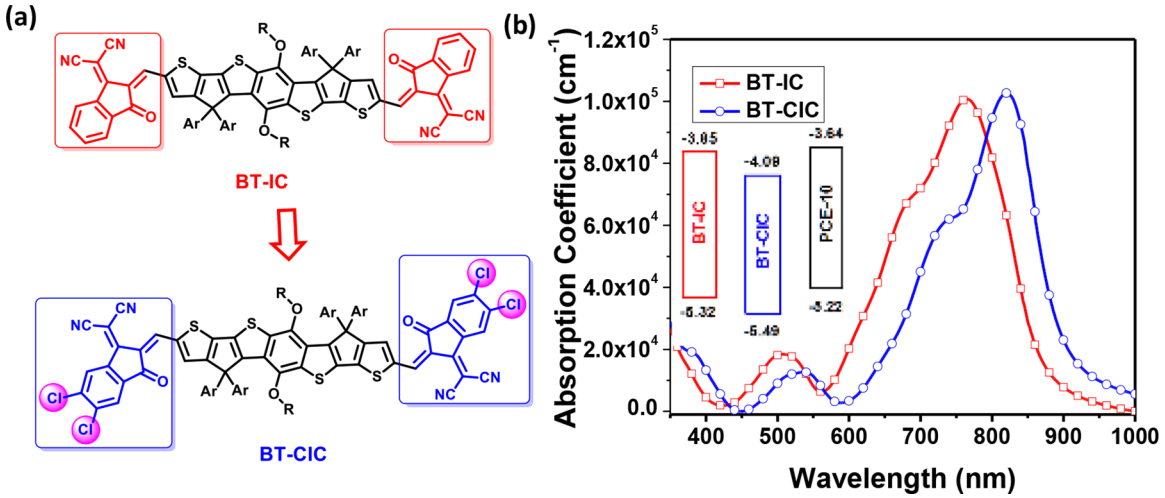

Figure 1. (a) Molecular structural formulas of BT-IC and BT-CIC and (b) UV−vis absorption spectra of BT-IC and BT-CIC thin films. Inset: Energy diagram of BT-IC, BT-CIC and PCE-10 relative to vacuum obtained from cyclic voltammetry.

to the large torsion angles between both of the π-bridges and the donor and acceptor units, the twisted molecular conformation led to a reduced charge mobility and fill factor (*FF*), thus reducing the *PCE*.

We recently developed a nonfullerene acceptor (4,4,10,10-tetrakis(4-hexylphenyl)-5,11-(2-ethylhexyloxy)-4,10-dihydro-dithienyl[1,2-b:4,5b′]benzodi-thiophene-2,8-diyl)bis(2-(3-oxo-2,3-dihydroinden-1-ylidene)malononitrile), BT-IC, that showed a planar structure with a torsion angle <1° and consequently, a high electron mobility.[13] However, the absorption of BT-IC does not extend to wavelengths λ > 850 nm. This leaves an unused part of the solar spectrum and a potential opening for further improvement in solar cell performance. Here, we demonstrate a new NFA molecular design concept that leads to a narrow absorption band confined to the NIR by the introduction of high electron affinity chlorine atoms (Pauline electronegativity for Cl: 3.16[14]). The electron acceptor, (4,4,10,10-tetrakis(4-hexylphenyl)-5,11-(2-ethylhexyloxy)-4,10-dihydro-dithienyl[1,2-b:4,5b′]benzodi-thiophene-2,8-diyl)bis-(2-(3-oxo-2,3-dihydroinden-5,6-dichloro-1-ylidene)-malononitrile), BT-CIC, comprises four chlorine atoms at the 5,6-positions of the 2-(3-oxo-2,3-dihydroinden-1-ylidene)-malononitrile. The design avoids significant issues of previously reported chlorinated molecules with nonspecific atomic site positioning (and hence property variability).[15] The Cl atoms effectively lower the energy gap by enhancing intramolecular charge transfer.[14,15] Moreover, the intermolecular interactions of Cl−S and Cl−Cl result in ordered molecular stacks in the donor−acceptor blend films.[16]

The BT-CIC molecule has an energy gap of ∼1.3 eV leading to an optical absorption edge at ∼1000 nm. Single-junction solar cells employing BT-CIC with a low energy gap polymer donor (poly[4,8-bis(5-(2-ethylhexyl)thiophen-2-yl)benzo[1,2-b:4,5-b′]dithiophene-*co*-3-fluorothieno[3,4-*b*]thio-phene-2-carboxylate], PCE-10) show *PCE* = 11.2 ± 0.4%, V_{oc} = 0.70 ± 0.01 V, short circuit current of J_{sc} = 22.5 ± 0.6 mA cm^{-2}, and *FF* = 71 ± 2% under 1 sun intensity (1 kW/m^2), simulated AM1.5G solar spectral illumination. To our knowledge, this is the highest efficiency reported for NIR organic solar cells. Our previous work on an analogous non-Cl containing molecule, BT-IC, achieved a high *PCE* by broadly harvesting the photons across the visible and NIR spectra, and hence there was little opportunity to engineer transparent OPVs suitable for BIPV applications. In contrast, the BT-CIC-based device can achieve *EQE* = 75% between the wavelengths of λ = 650 and 850 nm, leaving a transparency window between λ = 400 and 650 nm that allows for its use in efficient, semitransparent OPVs. The device using thin (10 nm) Ag cathodes shows *PCE* = 7.1 ± 0.1%, with an average visible transmittance (calculated from the simple arithmetic mean of the transmittances from 400 to 650 nm) of 43 ± 1.5%, Commission Internationale d'Eclairage (CIE) chromaticity coordinates of (0.29, 0.32) and a color rendering index of 91 when illuminated by a simulated, AM1.5G solar spectrum. These results open a new avenue for exploring highly efficient NIR solar cells by overcoming the challenge of synthesizing small energy gap organic materials leading to high device performance, and should accelerate the development of both very high efficiency tandem and semitransparent OPV cells.

RESULTS AND DISCUSSION

The molecular structural formulas of the two acceptors are shown in Figure 1a, which were prepared by Knoevenagel condensation reactions (see Supporting Information, SI). Both BT-IC and BT-CIC are soluble in tetrahydrofuran (THF), dichloromethane (DCM), chloroform (CF), chlorobenzene (CB), and *ortho*-dichlorobenzene (*o*-DCB), at room temperature. Thin film UV−vis absorption spectra of BT-IC and BT-CIC are shown in Figure 1b. BT-CIC absorbs between λ = 650 and 1000 nm while being transparent in the visible, with an optical bandgap of 1.33 eV as determined from the absorption onset at λ = 930 nm. Importantly, BT-CIC exhibits a bathochromic shift of ∼60 nm compared to BT-IC, which suggests increased internal charge transfer. The maximum absorption coefficient of the BT-CIC film (1.03 ± 0.03 × 10^5 cm^{-1}) at λ = 820 nm is similar to that of BT-IC (1.00 ± 0.04 × 10^5 cm^{-1}) at the shorter wavelength of λ = 765 nm.

Cyclic voltammetry in Figure S1 in SI was used to obtain the highest occupied (HOMO) and the lowest unoccupied molecular orbital (LUMO) energies (E_{HOMO} and E_{LUMO}, respectively) of −5.32 (±0.03) and −3.85 (±0.02) eV, respectively, for BT-IC, and −5.49 (±0.02) and −4.09 (±0.02) eV, respectively, for BT-CIC. BT-CIC shows a lower HOMO−LUMO energy gap (1.40 eV) than BT-IC (1.47 eV),

DOI: 10.1021/jacs.7b11278
J. Am. Chem. Soc. 2017, 139, 17114−17119

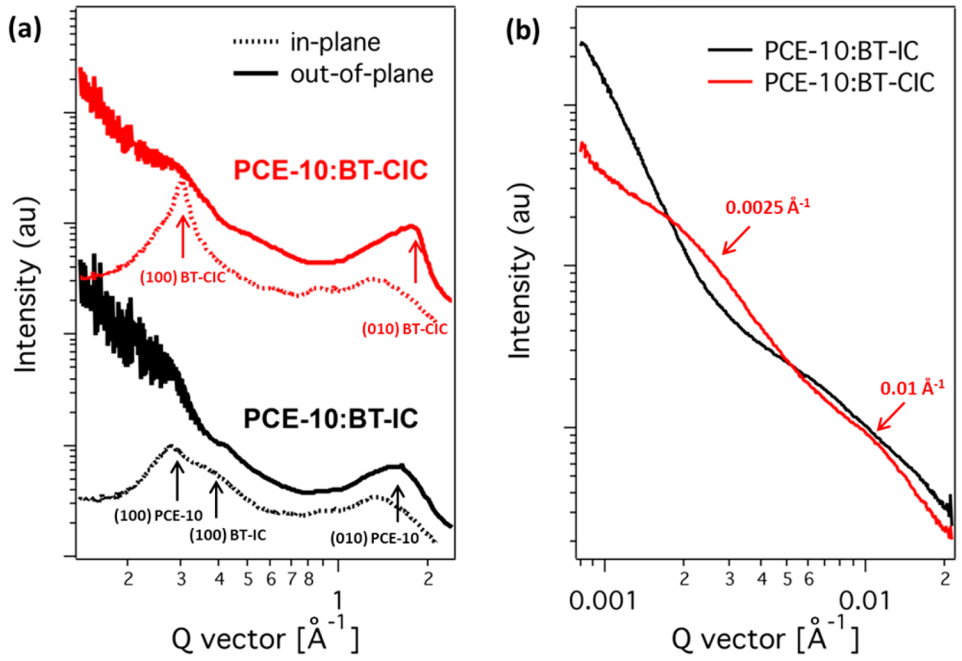

Figure 2. (a) In-plane (dotted line) and out-of-plane (solid line) X-ray scattering patterns extracted from 2D grazing incidence X-ray diffraction (GIXD) of PCE-10:BT-IC and PCE-10:BT-CIC blends, and (b) resonant soft X-ray diffraction of PCE-10:BT-IC and PCE-10:BT-CIC blends. Here, Q is the scattering vector.

which is consistent with experimental results from the optical measurements. BT-CIC exhibits both lower HOMO and LUMO energies compared with BT-IC due to the electron-withdrawing ability of the Cl atoms in the former molecule. The lower E_{LUMO} leads to increased chemical stability and improved electron injection efficiency as the Schottky barrier with the cathode contact is decreased.[13]

Density functional theory (DFT) at the B3LYP/6-31G(d) level was used to investigate the geometric and electronic properties of BT-IC and BT-CIC. Both molecules have a planar structure with a torsion angle <1° (see Figure S2), which differs from previously reported small energy gap NFAs with twisted backbones. The planar geometry facilitates π-electron delocalization and enhances both the charge mobility and *FF*.[17] This also implies that Cl-containing BT-CIC presents a small steric hindrance originating from the large size of Cl atoms in contrast with the H-containing molecule BT-IC. Moreover, the larger electron densities on the S atoms in BT-IC and BT-CIC compared to the indaceno[1,2-b:5,6-b′]dithieno[3,2-*b*]-thiophene based molecules result in substantial overlap between neighboring molecules in the solid state, giving rise to increased crystalline order.[10m]

To better understand charge transport properties of the films, the morphologies of both the neat films (see in Figure S3) and blends were characterized by glancing incidence X-ray diffraction. The (100) diffraction peak of PCE-10:BT-IC in Figures 2a and S4 at 0.28 Å^{-1} with a crystal correlation length of ζ = 7.7 ± 0.2 nm is due to PCE-10, which is partially merged with the BT-IC (100) diffraction peak at 0.38 Å^{-1} with ζ = 4.2 ± 0.1 nm. The (010) diffraction peak of PCE-10:BT-IC blend, particularly in the out-of-plane direction, is dominated by the contribution from PCE-10 because the (010) peak is located at 1.6 Å^{-1}. In this case, PCE-10 guides the blend morphology. In contrast, the PCE-10:BT-CIC blend shows a (010) peak in the out-of-plane direction at ∼1.8 Å^{-1}, characteristic of BT-CIC. Chlorination also causes a significant increase in (100) intensity, a larger aggregate size of ζ = 17.9 ± 0.4 nm, and a smaller (100) spacing than for the PCE-10:BT-IC blend.

Phase separation of the blends was studied by resonant soft X-ray diffraction with scattering profiles shown in Figure 2b. The PCE-10:BT-IC blend shows a single diffuse peak over a scattering parameter range of Q = 0.004 to 0.02 Å^{-1}, suggesting structure at a dimension of hundreds of nanometers. In contrast, a multilength-scale morphology was observed in the PCE-10:BT-CIC blend, with one peak at Q = 0.01 Å^{-1} (corresponding to a distance of 63 nm) and another at 0.0025 Å^{-1} (250 nm). The smaller length scale results from PCE-10 and/or BT-CIC nanocrystalline aggregates, whereas the larger arises from PCE-10- and BT-CIC-rich domains that comprise aggregates embedded in an amorphous matrix. Atomic force microscopy (AFM) images of two blends are shown in Figure S5. The PCE-10:BT-CIC blend has a root-mean-square roughness of 0.97 nm, compared with 3.20 nm for the PCE-10:BT-IC blend.

The charge generation process begins with exciton migration to a donor−acceptor heterojunction.[18] The order and close π-stacking in the PCE-10:BT-CIC blend which is driven by the chloride functional groups results in nanocrystallites of several tens to hundreds of nanometers. This, in turn increases the diffusion length of the excitons while also decreasing the resistance to the conduction of liberated charges to their corresponding electrodes.[19] For example, hole and electron mobilities of 6.5 ± 0.2 × 10^{-4} and 2.1 ± 0.1 × 10^{-4} cm^2 V^{-1} s^{-1}, respectively, were found for the PCE-10:BT-CIC blend based on analysis of space charge limited current of the thin films (see Figures S6−S9). This is compared to 5.1 ± 0.3 × 10^{-4} and 1.2 ± 0.1 × 10^{-4} cm^2 V^{-1} s^{-1} for the PCE-10:BT-IC blend. The high electron mobilities result in efficient charge extraction from donor−acceptor junctions. The details of these measurements are found in Methods (SI).

On the basis of these morphological results, we can understand the performance of OPVs based on BT-IC and

DOI: 10.1021/jacs.7b11278
J. Am. Chem. Soc. 2017, 139, 17114−17119

Table 1. Operating characteristics of OPVs under simulated AM 1.5G, 100 mW cm^{-2} illumination

Acceptor[a]	J_{sc}[b] [mA/cm^2]	V_{oc} [V]	*FF* [%]	*PCE*[c] [%]
$PC_{71}BM$	17.9 ± 0.4 (17.5)	0.80 ± 0.01	69.3 ± 1.3	9.6 ± 0.3
BT-IC	17.5 ± 0.4 (16.7)	0.81 ± 0.01	59.6 ± 1.5	8.3 ± 0.2
BT-CIC	22.5 ± 0.6 (21.3)	0.70 ± 0.01	71.0 ± 1.9	11.2 ± 0.4

[a]All blends are donor:acceptor 1:1.5. The donor is PCE-10. [b]The values in parentheses are calculated from the integral of the *EQE* spectrum. [c]The average value is based on measurements of 20 devices.

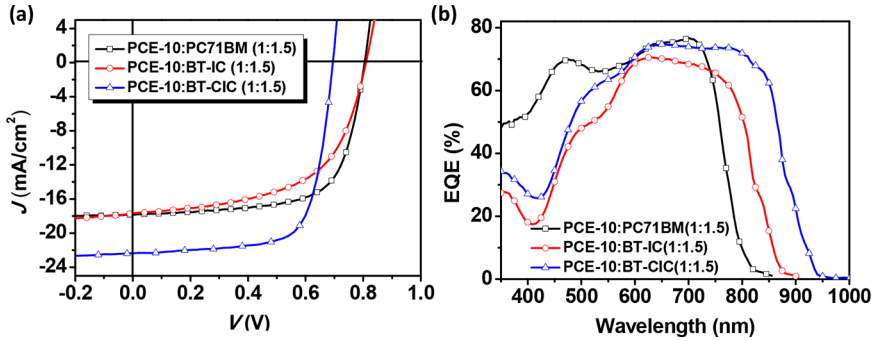

Figure 3. (a) Current-density−voltage characteristics, and (b) external quantum efficiency (*EQE*) spectra of organic photovoltaic cells based on PCE-10:$PC_{71}BM$ (1:1.5, w/w), PCE-10:BT-IC (1:1.5, w/w), and PCE-10:BT-CIC (1:1.5, w/w).

Table 2. Operating Characteristics of Semitransparent PCE-10:BT-CIC OPVs with Different Ag Cathode Thicknesses under Simulated AM 1.5G, 100 mW cm^{-2} Illumination

Ag Thickness [nm]	J_{sc}[a] [mA/cm^2]	V_{oc} [V]	*FF* [%]	*PCE*[b] [%]	*AVT* [%]	R_{series} [Ω cm^2]	R_{sheet} [Ω/sq]
10	15.8 ± 0.1 (15.2)	0.68 ± 0.01	66.2 ± 1.2	7.1 ± 0.1	43 ± 1.5	2.1 ± 0.1	28.0 ± 1.2
15	17.0 ± 0.3 (16.0)	0.68 ± 0.01	67.1 ± 0.9	7.7 ± 0.1	33 ± 1.1	1.7 ± 0.1	4.3 ± 0.3
20	18.0 ± 0.3 (17.1)	0.68 ± 0.01	67.5 ± 1.8	8.2 ± 0.2	26 ± 0.5	1.7 ± 0.1	2.4 ± 0.5

[a]The values in parentheses are calculated from the integral of the *EQE* spectrum. [b]The average value is based on measurements of 8 devices.

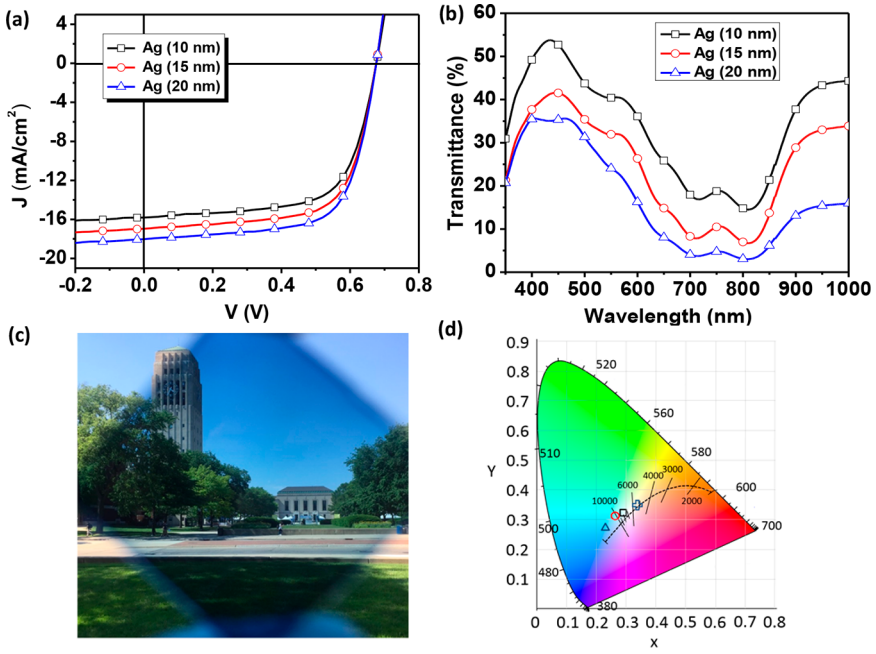

Figure 4. (a) Current-density−voltage characteristics of semitransparent OPVs (STOPVs) based on PCE-10:BT-CIC (1:1.5, w/w) with different Ag cathode thicknesses. (b) Transmission spectra of the corresponding STOPVs with different Ag thicknesses. (c) Outdoor image through the STOPV incorporating a 10 nm thick Ag layer, and (d) CIE coordinates of the transmission spectra of devices with different Ag thicknesses using a AM1.5G solar simulated input spectrum (denoted by '+'), 10 nm thick Ag ('□' square), 15 nm Ag ('○' circle), and 20 nm Ag ('△' triangle).

BT-CIC. The OPVs had device structures of: indium tin oxide (ITO)/ZnO (25 nm)/PCE-10 mixed with BT-IC or BT-CIC (130 nm)/MoO_3 (15 nm) /Ag (100 nm). The details of fabrication are found in Methods (SI). The current-density−voltage (*J*−*V*) characteristics are plotted in Figure 3a, with the detailed device parameters summarized in Table 1. For

DOI: 10.1021/jacs.7b11278
J. Am. Chem. Soc. 2017, 139, 17114−17119

comparison, we fabricated OPVs with analogous structures based on PCE-10:$PC_{71}BM$. The optimized devices for PCE-10:BT-IC or BT-CIC were spin-coated from 9:1 chlorobenzene:chloroform solution mixed with a 1:1.5 donor:acceptor (D:A) weight ratio. The highest $PCE = 11.2 \pm 0.4\%$ was achieved in the BT-CIC-based device, with $V_{oc} = 0.70 \pm 0.01$ V, $J_{sc} = 22.5 \pm 0.6$ mA cm^{-2}, and $FF = 0.71 \pm 0.02$ under a simulated AM1.5G, one sun intensity solar spectrum. In contrast, the BT-IC-based OPV exhibited $PCE = 8.3 \pm 0.2\%$ with $V_{oc} = 0.81 \pm 0.01$ V, $J_{sc} = 17.5 \pm 0.4$ mA cm^{-2}, and $FF = 0.60 \pm 0.02$. For the PCE-10:$PC_{71}BM$ device, $PCE = 9.6 \pm 0.3\%$ with $V_{oc} = 0.80 \pm 0.01$ V, $J_{sc} = 17.9 \pm 0.4$ mA cm^{-2}, and $FF = 0.69 \pm 0.01$.

The significant improvement in J_{sc} for the BT-CIC OPV is attributed to its red-shifted absorption that provides solar spectral response into the NIR, and its improved stacking leading to large and ordered aggregates compared to the other NFA. The *EQE* vs wavelength spectrum is shown in Figure 3b. The long wavelength cutoff of BT-CIC at $\lambda = 950$ nm is red-shifted by ∼80 nm compared to BT-IC, and ∼170 nm compared to $PC_{71}BM$. The *EQE* of the BT-CIC OPV reaches 75%, between $\lambda = 650$ and 850 nm. The integrated $J_{sc} = 21.3$ mA cm^{-2} is within 5% of the solar simulation measurement.

A transparency window between the visible wavelengths of 400 and 650 nm for the BT-CIC OPV was exploited in semitransparent OPVs (STOPVs) with the structure: ITO/ZnO (18 nm)/PCE-10: BT-CIC (120 nm)/MoO_3 (15 nm)/Ag (x). To determine the trade-off between transparency and efficiency, STOPVs with Ag thicknesses of $x = 10$, 15, and 20 nm were fabricated. The $J-V$, transmission, and *EQE* spectral characteristics for the devices are shown in Figures 4 and Figures S10−S11, and the results are summarized in Table 2 and Table S1. The average visible transmittance (*AVT*) of the devices, which is calculated from the simple arithmetic mean of the transmittances from 400 to 650 nm, varied from $26 \pm 0.5\%$ to $43 \pm 1.5\%$, with 20 nm $\geq x \geq$ 10 nm. For $x = 10$ nm, the STOPV showed $PCE = 7.1 \pm 0.1\%$, and for $x = 20$ nm, $PCE = 8.2 \pm 0.2$, which are measured from ITO side with no object behind the cells. The J_{sc} significantly decreased compared to the opaque devices due to the reduced reflectivity of the thin cathode, leading to the lower light intensity within the active layer. A decreased V_{oc} and *FF* were also found in the STOPVs due to increased sheet resistance of the thin Ag electrodes.[20] Figure 4c shows a photograph of a semitransparent OPV covered by the 10 nm thick Ag layer.

Semitransparent OPVs have potential applications as power-generating windows for buildings and automobiles. Hence, their visual appearance must also be quantified.[21] The device appearance was examined using AM1.5G simulated solar illumination. The 1931 CIE chromaticity coordinates are shown in Figure 4d. The transmitted light of the device with a 10 nm thick Ag cathode has color coordinates of (0.29, 0.32), which is close to the D75 standard illuminant (a white light source with color rendering index of $CRI = 100$ and correlated color temperature of $CCT = 7500$ K). The STOPV also exhibited $CRI = 91$ and $CCT = 7784$ K. This high CRI indicates that the illumination through the OPV window can accurately render the color of an object, giving it only a slightly bluish tint.

Although ultrathin metal films have been successfully demonstrated in STOPVs, their use may nevertheless limit their application to large-scale windows, possibly due to the discontinuous and resistive films, or poor contact between the interfacial layer and electrode. Therefore, developing other transparent electrodes with high transparency, low resistance and effective charge collection, represents a high value problem.[8a]

CONCLUSIONS

In summary, we developed an NIR-absorbing nonfullerene acceptor (BT-CIC) featuring four chloride atoms at defined molecular sites. The significant impacts of chlorination on electronic structures, crystal properties, and the morphology of the NFAs have been determined. We find that site-specific chlorination is a powerful route toward achieving high performance NIR solar cells. Considering the synthetic accessibility and lower cost of chloro-containing precursors compared to the well-developed fluorinated molecules, this work provides new avenues in the design of NIR acceptors. Moreover, the BT-CIC-based single-junction solar cells achieve $PCE = 11.2 \pm 0.4\%$, $J_{sc} = 22.5 \pm 0.6$ mA cm^{-2}, $V_{oc} = 0.70 \pm 0.01$ V, and $FF = 0.71 \pm 0.02$. This performance was achieved only by selectively harvesting the photons from the NIR region. Importantly, the *EQE* of the BT-CIC-based device reaches 75%, between 650 and 850 nm while leaving a transparency window between 400 and 650 nm. These results indicate that BT-CIC and other Cl-based molecules are effective for use in NIR solar cells with applications to semitransparent and tandem solar cells for BIPV.

ASSOCIATED CONTENT

Supporting Information

The Supporting Information is available free of charge on the ACS Publications website at DOI: 10.1021/jacs.7b11278.

Experiment details, calculations (PDF)

AUTHOR INFORMATION

Corresponding Authors

*stevefor@umich.edu

*lsliao@suda.edu.cn

ORCID

Liang-Sheng Liao: 0000-0002-2352-9666

Stephen R. Forrest: 0000-0003-0131-1903

Notes

The authors declare no competing financial interest.

ACKNOWLEDGMENTS

Y.L. and S.R.F. were funded in part by the Office of Energy Efficiency and Renewable Energy (EERE), U.S. Department of Energy, under Award Number DE-EE0006708 and by the Department of the Navy, Office of Naval Research under Award No. N00014-17-1-2211. GIXD measurements were carried out at beamline 7.3.3 and 11.0.1.2 at the Advanced Light Source, and Molecular Foundry, Lawrence Berkeley National Laboratory, which was supported by the U.S. Department of Energy, Offices of Science, and Basic Energy Sciences. This work was also supported by the National Natural Science Foundation of China (21504062) and the Collaborative Innovation Centre of Suzhou Nano Science and Technology (Nano-CIC).

REFERENCES

(1) Forrest, S. R. *Nature* **2004**, *428*, 911.

(2) (a) Peumans, P.; Uchida, S.; Forrest, S. R. *Nature* **2003**, *425*, 158. (b) Yu, G.; Gao, J.; Hummelen, J. C.; Wudl, F.; Heeger, A. J. *Science*

DOI: 10.1021/jacs.7b11278
J. Am. Chem. Soc. 2017, 139, 17114−17119

1995, *270*, 1789. (c) Peumans, P.; Forrest, S. R. *Appl. Phys. Lett.* **2001**, *79*, 126.
(3) (a) Che, X.; Xiao, X.; Zimmerman, J. D.; Fan, D.; Forrest, S. R. *Adv. Energy Mater.* **2014**, *4*, 1400568. (b) Zhao, J.; Li, Y.; Yang, G.; Jiang, K.; Lin, H.; Ade, H.; Ma, W.; Yan, H. *Nat. Energy* **2016**, *1*, 15027. (c) Chen, C.-C.; Chang, W.-H.; Yoshimura, K.; Ohya, K.; You, J.; Gao, J.; Hong, Z.; Yang, Y. *Adv. Mater.* **2014**, *26*, 5670.
(4) (a) Janssen, R. A. J.; Nelson, J. *Adv. Mater.* **2013**, *25*, 1847. (b) Hendriks, K. H.; Li, W.; Wienk, M. M.; Janssen, R. A. J. *J. Am. Chem. Soc.* **2014**, *136*, 12130. (c) Servaites, J. D.; Ratner, M. A.; Marks, T. J. *Energy Environ. Sci.* **2011**, *4*, 4410. (d) Li, W.; Hendriks, K. H.; Furlan, A.; Wienk, M. M.; Janssen, R. A. J. *J. Am. Chem. Soc.* **2015**, *137*, 2231. (e) Kawashima, K.; Tamai, Y.; Ohkita, H.; Osaka, I.; Takimiya, K. *Nat. Commun.* **2015**, *6*, 10085.
(5) (a) Dou, L.; You, J.; Yang, J.; Chen, C.-C.; He, Y.; Murase, S.; Moriarty, T.; Emery, K.; Li, G.; Yang, Y. *Nat. Photonics* **2012**, *6*, 180. (b) Ameri, T.; Li, N.; Brabec, C. J. *Energy Environ. Sci.* **2013**, *6*, 2390. (c) Li, G.; Chang, W.-H.; Yang, Y. *Nat. Rev. Mater.* **2017**, *2*, 17043.
(6) (a) You, J.; Dou, L.; Yoshimura, K.; Kato, T.; Ohya, K.; Moriarty, T.; Emery, K.; Chen, C. C.; Gao, J.; Li, G.; Yang, Y. *Nat. Commun.* **2013**, *4*, 1446. (b) Li, Y.; Zou, J.; Yip, H.-L.; Li, C.-Z.; Zhang, Y.; Chueh, C.-C.; Intemann, J.; Xu, Y.; Liang, P.-W.; Chen, Y.; Jen, A. K. Y. *Macromolecules* **2013**, *46*, 5497.
(7) Dou, L.; Liu, Y.; Hong, Z.; Li, G.; Yang, Y. *Chem. Rev.* **2015**, *115*, 12633.
(8) (a) Chen, C.-C.; Dou, L.; Zhu, R.; Chung, C.-H.; Song, T.-B.; Zheng, Y. B.; Hawks, S.; Li, G.; Weiss, P. S.; Yang, Y. *ACS Nano* **2012**, *6*, 7185. (b) Min, J.; Bronnbauer, C.; Zhang, Z.-G.; Cui, C.; Luponosov, Y. N.; Ata, I.; Schweizer, P.; Przybilla, T.; Guo, F.; Ameri, T.; Forberich, K.; Spiecker, E.; Bäuerle, P.; Ponomarenko, S. A.; Li, Y.; Brabec, C. J. *Adv. Funct. Mater.* **2016**, *26*, 4543. (c) Chang, C.-Y.; Zuo, L.; Yip, H.-L.; Li, Y.; Li, C.-Z.; Hsu, C.-S.; Cheng, Y.-J.; Chen, H.; Jen, A. K. Y. *Adv. Funct. Mater.* **2013**, *23*, 5084. (d) Betancur, R.; Romero-Gomez, P.; Martinez-Otero, A.; Elias, X.; Maymo, M.; Martorell, J. *Nat. Photonics* **2013**, *7*, 995.
(9) (a) Nielsen, C. B.; Holliday, S.; Chen, H.-Y.; Cryer, S. J.; Mcculloch, I. *Acc. Chem. Res.* **2015**, *48*, 2803. (b) Lin, Y.; Zhan, X. *Mater. Horiz.* **2014**, *1*, 470. (c) Li, Y.; Gu, M.; Pan, Z.; Zhang, B.; Yang, X.; Gu, J.; Chen, Y. *J. Mater. Chem. A* **2017**, *5*, 10798.
(10) (a) Lin, Y.; Wang, J.; Zhang, Z.-G.; Bai, H.; Li, Y.; Zhu, D.; Zhan, X. *Adv. Mater.* **2015**, *27*, 1170. (b) Lin, Y.; Zhang, Z.-G.; Bai, H.; Wang, J.; Yao, Y.; Li, Y.; Zhu, D.; Zhan, X. *Energy Environ. Sci.* **2015**, *8*, 610. (c) Li, S.; Ye, L.; Zhao, W.; Zhang, S.; Mukherjee, S.; Ade, H.; Hou, J. *Adv. Mater.* **2016**, *28*, 9423. (d) Liu, F.; Zhou, Z.; Zhang, C.; Vergote, T.; Fan, H.; Liu, F.; Zhu, X. *J. Am. Chem. Soc.* **2016**, *138*, 15523. (e) Kan, B.; Feng, H.; Wan, X.; Liu, F.; Ke, X.; Wang, Y.; Wang, Y.; Zhang, H.; Li, C.; Hou, J.; Chen, Y. *J. Am. Chem. Soc.* **2017**, *139*, 4929. (f) Liu, Y.; Mu, C.; Jiang, K.; Zhao, J.; Li, Y.; Zhang, L.; Li, Z.; Lai, J. Y. L.; Hu, H.; Ma, T.; Hu, R.; Yu, D.; Huang, X.; Tang, B. Z.; Yan, H. *Adv. Mater.* **2015**, *27*, 1015. (g) Holliday, S.; Ashraf, R. S.; Nielsen, C. B.; Kirkus, M.; Röhr, J. A.; Tan, C.-H.; Collado-Fregoso, E.; Knall, A.-C.; Durrant, J. R.; Nelson, J.; McCulloch, I. *J. Am. Chem. Soc.* **2015**, *137*, 898. (h) Holliday, S.; Ashraf, R. S.; Wadsworth, A.; Baran, D.; Yousaf, S. A.; Nielsen, C. B.; Tan, C.-H.; Dimitrov, S. D.; Shang, Z.; Gasparini, N.; Alamoudi, M.; Laquai, F.; Brabec, C. J.; Salleo, A.; Durrant, J. R.; McCulloch, I. *Nat. Commun.* **2016**, *7*, 11585. (i) Hwang, Y.-J.; Li, H.; Courtright, B. A. E.; Subramaniyan, S.; Jenekhe, S. A. *Adv. Mater.* **2016**, *28*, 124. (j) Zhao, W.; Li, S.; Yao, H.; Zhang, S.; Zhang, Y.; Yang, B.; Hou, J. *J. Am. Chem. Soc.* **2017**, *139*, 7148. (k) Lin, Y.; He, Q.; Zhao, F.; Huo, L.; Mai, J.; Lu, X.; Su, C.-J.; Li, T.; Wang, J.; Zhu, J.; Sun, Y.; Wang, C.; Zhan, X. *J. Am. Chem. Soc.* **2016**, *138*, 2973. (l) Dai, S.; Zhao, F.; Zhang, Q.; Lau, T.-K.; Li, T.; Liu, K.; Ling, Q.; Wang, C.; Lu, X.; You, W.; Zhan, X. *J. Am. Chem. Soc.* **2017**, *139*, 1336. (m) Li, Y.; Zhong, L.; Lin, J.-D.; Wu, F.-P.; Bin, H.-J.; Zhang, Z.; Xu, L.; Jiang, Z.-Q.; Zhang, Z.-G.; Liu, F.; Russell, T. P.; Li, Y.; Liao, L.-S.; Forrest, S. R. *Solar RRL* **2017**, *1*, 1700107. (n) Yang, Y.; Zhang, Z.-G.; Bin, H.; Chen, S.; Gao, L.; Xue, L.; Yang, C.; Li, Y. *J. Am. Chem. Soc.* **2016**, *138*, 15011. (o) Feng, S.; Zhang, C. e.; Liu, Y.; Bi, Z.; Zhang, Z.; Xu, X.; Ma, W.; Bo, Z. *Adv. Mater.* **2017**, *29*, 1703527. (p) Zhang, H.; Wang, X.; Yang, L.; Zhang, S.; Zhang, Y.; He, C.; Ma, W.; Hou, J. *Adv. Mater.* **2017**, *29*, 1703777. (q) Xu, S. j.; Zhou, Z.; Liu, W.; Zhang, Z.; Liu, F.; Yan, H.; Zhu, X. *Adv. Mater.* **2017**, DOI: 10.1002/adma.201704510.
(11) (a) Yao, H.; Chen, Y.; Qin, Y.; Yu, R.; Cui, Y.; Yang, B.; Li, S.; Zhang, K.; Hou, J. *Adv. Mater.* **2016**, *28*, 8283. (b) Wang, W.; Yan, C.; Lau, T.-K.; Wang, J.; Liu, K.; Fan, Y.; Lu, X.; Zhan, X. *Adv. Mater.* **2017**, *29*, 1701308.
(12) (a) Yao, H.; Cui, Y.; Yu, R.; Gao, B.; Zhang, H.; Hou, J. *Angew. Chem., Int. Ed.* **2017**, *56*, 3045. (b) Liu, F.; Zhou, Z.; Zhang, C.; Zhang, J.; Hu, Q.; Vergote, T.; Liu, F.; Russell, T. P.; Zhu, X. *Adv. Mater.* **2017**, *29*, 1606574.
(13) Li, Y.; Zhong, L.; Gautam, B.; Bin, H.-J.; Lin, J.-D.; Wu, F.-P.; Zhang, Z.; Jiang, Z.-Q.; Zhang, Z.-G.; Gundogdu, K.; Li, Y.; Liao, L.-S. *Energy Environ. Sci.* **2017**, *10*, 1610.
(14) Tang, M. L.; Oh, J. H.; Reichardt, A. D.; Bao, Z. *J. Am. Chem. Soc.* **2009**, *131*, 3733.
(15) (a) Mo, D.; Wang, H.; Chen, H.; Qu, S.; Chao, P.; Yang, Z.; Tian, L.; Su, Y.-A.; Gao, Y.; Yang, B.; Chen, W.; He, F. *Chem. Mater.* **2017**, *29*, 2819. (b) Qu, S.; Wang, H.; Mo, D.; Chao, P.; Yang, Z.; Li, L.; Tian, L.; Chen, W.; He, F. *Macromolecules* **2017**, *50*, 4962. (c) Yang, F.; Li, C.; Lai, W.; Zhang, A.; Huang, H.; Li, W. *Mater. Chem. Front.* **2017**, *1*, 1389.
(16) (a) Lei, T.; Dou, J.-H.; Ma, Z.-J.; Liu, C.-J.; Wang, J.-Y.; Pei, J. *Chem. Sci.* **2013**, *4*, 2447. (b) Zheng, Y.-Q.; Wang, Z.; Dou, J.-H.; Zhang, S.-D.; Luo, X.-Y.; Yao, Z.-F.; Wang, J.-Y.; Pei, J. *Macromolecules* **2015**, *48*, 5570.
(17) Li, Y.; Yao, K.; Yip, H.-L.; Ding, F.-Z.; Xu, Y.-X.; Li, X.; Chen, Y.; Jen, A. K. Y. *Adv. Funct. Mater.* **2014**, *24*, 3631.
(18) Chen, W.; Xu, T.; He, F.; Wang, W.; Wang, C.; Strzalka, J.; Liu, Y.; Wen, J.; Miller, D. J.; Chen, J.; Hong, K.; Yu, L.; Darling, S. B. *Nano Lett.* **2011**, *11*, 3707.
(19) Lunt, R. R.; Benziger, J. B.; Forrest, S. R. *Adv. Mater.* **2007**, *19*, 4229.
(20) Chueh, C.-C.; Chien, S.-C.; Yip, H.-L.; Salinas, J. F.; Li, C.-Z.; Chen, K.-S.; Chen, F.-C.; Chen, W.-C.; Jen, A. K. Y. *Adv. Energy Mater.* **2013**, *3*, 417.
(21) Chen, K.-S.; Salinas, J.-F.; Yip, H.-L.; Huo, L.; Hou, J.; Jen, A. K. Y. *Energy Environ. Sci.* **2012**, *5*, 9551.

DOI: 10.1021/jacs.7b11278
J. Am. Chem. Soc. 2017, 139, 17114−17119